Simulations of a rotor with active deformable trailing edge flaps in half-wake inflow: Comparison of EllipSys 3D with HAWC2

Thanasis Barlas, Frederik Zahle, Niels N. Sørensen, Mac Gaunaa, and Leonardo Bergami

Aeroelastic Design, DTU Wind Energy, DTU Risø Campus, Denmark

Abstract

Various research projects have focused on active aerodynamic load control of wind turbines using control devices on the blades, for example flaps. The aerodynamic load predictions of utilized aeroelastic codes have not yet been fully validated with full rotor CFD or experimental results. In this study, a comparison between aerodynamic predictions of the aeroelastic code HAWC2 and the Navier-Stokes code EllipSys3D for the NREL 5MW reference wind turbine rotor in a stiff configuration equipped with a deformable trailing edge flap is performed. A case where the half rotor plane experiences an inflow resembling the wake from an upstream wind turbine is investigated, which is appropriate for comparing the predictions of the two codes related to the abrupt aerodynamic response and the influence of the controllable flap. The trailing edge flap is actuated to alleviate the added loads from a non-uniform inflow mimicking a half-wake situation, using different control methods and maximum flap angles. Three different control inputs are simulated: a prescribed flap angle based on the a priori knowledge of the inflow velocity, a controller based on the blade root flap-wise moment feedback, and finally a controller based on a Pitot tube velocity feedback measured at flap mid-span. Good agreement is found between EllipSys3D and HAWC2 in the prediction of the dynamic blade loads, considering the high complexity of the flow case.

Keywords

rotor, active deformable trailing edge flaps, half-wake, CFD

1. Introduction

The size of wind turbines has been increasing rapidly over the past years. Rotors of more than 120m diameter are already commercially available, and prototypes with a rotor diameter of more than 160m are designed. Focusing on lowering the cost per kWh, new trends and technological improvements have been primary targets of research and development. One main focus is on developing new technologies capable of considerably reducing fatigue loads
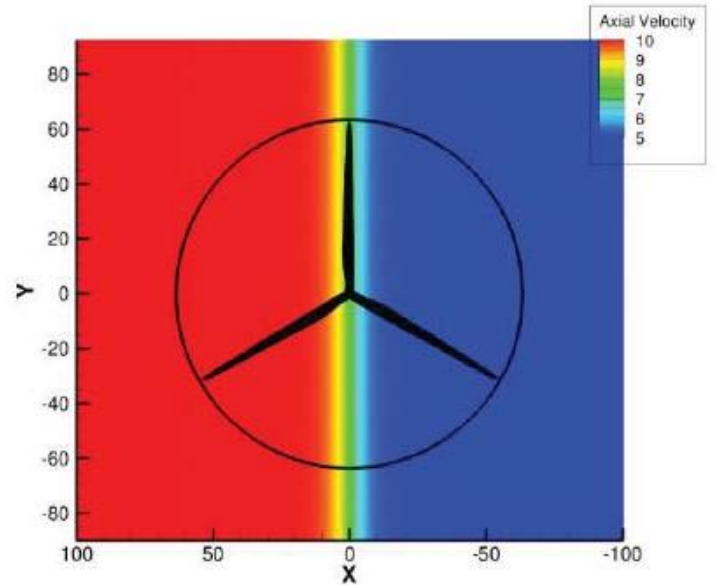
on wind turbines. New concepts for dynamic load reduction are focusing on a much faster and detailed load control, compared to existing individual blade pitch control, by utilizing active aerodynamic control devices distributed along the blade span. So far, results from numerical and experimental analysis mostly focusing on trailing edge flaps, have shown a considerable potential in fatigue load reduction. The focus of this article is to investigate the validity of the aerodynamic predictions of a BEM-based aeroelastic tool compared to full rotor CFD simulations in a 3D rotor environment combined with extreme inflow changes and flap activation.

2. Half-wake inflow

The `half-wake´ ideally resembles the inflow conditions of a case where the rotor experiences a wake of an upstream wind turbine passing through the right side of the rotor disc, when looking downstream. Although idealized fin terms of abrupt deficit jump (in order to evaluate the code performance in an extreme case), this is a realistic situation during wind turbine operation in wind farms. The deficit with half the velocity compared to the undisturbed flow is common and not the most extreme wake inflow case [21]. This special inflow is modeled as a user-defined shear in HAWC2, which can be seen in Figure 1. The inflow presents 10 m/s at left side 5 m/s at right side seen from upstream, with a smooth transition between normal inflow and half-wake velocity

$$V = V_{max}\left(0.75 - 0.25\left(\tanh-8.78044\frac{x}{R}\right)\right)$$

(1)

where x is the lateral coordinate in the rotor plane, and R is the rotor radius. The 12.6m long and 10%c flap is located between 47.25m and 59.85m from the rotor axis. The simulated maximum flap angles are ±5 deg. The rotor operates at constant speed of ω=0.92 rad/s.

Figure 1 - The half-wake inflow with 10 m/s on the left side and 5 m/s on the right side of the rotor, viewed from an upstream location.

3. Modeling Approach and test cases

The NREL 5MW Reference Wind Turbine (RWT) [17] is used for the simulations, as a representative modern multi-MW wind turbine model which has been used extensively for active controls studies. The Computational Fluid Dynamics (CFD) code EllipSys 3D and the aeroelastic code HAWC2 are utilized in order to simulate the investigated case of a 3D rotor in a half-wake inflow, together with flap controls. In EllipSys only the exact 3D geometry of the rotor and the flaps, and the operating conditions (including the inflow definition) are modeled. In HAWC2, the geometry definition is simpler but there is need for airfoil data (including the flap effects) and additional assumptions. One, 20% of blade span, flap per blade is modeled, extending from 47.25m until 59.85m from the rotor axis. The rotor is rotating with a constant speed of 0.92 rad/s. The flap is located at the tip sections of the blade, where the NACA64618

airfoil is used with a smooth 10% chord-wise length deformable trailing edge flap.

3.1 EllipSys

All CFD computations in this study were carried out using the flow solver EllipSys3D developed by Michelsen [10, 11] and Sørensen [14]. The EllipSys3D solver is a multiblock finite volume discretization of the incompressible Reynolds-averaged Navier-Stokes (RANS) equations in general curvilinear coordinates. The variables are stored in a collocated grid arrangement, and odd/even pressure decoupling is avoided using the Rhie-Chow interpolation [13]. To solve the coupled momentum and pressure-correction equations the iterative SIMPLE [12] or PISO [5] algorithms are used. For unsteady simulations the solution is advanced in time using a second order iterative time-stepping (or dual time stepping) method. The convective terms are discretized using the Quadratic Upstream Interpolation for Convective Kinematics Scheme, QUICK [7], and the viscous terms are discretized using the central difference scheme. To accelerate the convergence of the pressure-correction equation a multigrid solution strategy is implemented and the code is fully parallelized using the MPI library. To further accelerate the convergence of the solution, grid and time step sequencing is used. In each level in the grid sequence every second grid point is removed, reducing the number of cells by a factor eight.

To handle the relative motion between the rotor and the ground the so-called overset grid method is used. In the present implementation by Zahle [16] each group of simply connected blocks is solved using boundary conditions on the overlapping interfaces based on interpolated values of velocity from neighboring grids using trilinear interpolation. An explicit correction of the conservation error associated with the non-conservative interpolation is implemented, since a divergence free field is required to solve the pressure-correction equation. The correction is placed in internal cells along the overset boundaries and is distributed proportionally to the local mass flux. The solution of the pressure is obtained on the basis of the mass fluxes calculated from the momentum equations.

To generate the deformable trailing edges for a blade section or a rotor, a total of three surface geometries were generated. One undeflected shape as well as two additional surface geometries; one with the trailing edge deflected downwards along the entire span, and another with the trailing edge deflected upwards. The trailing edge deformation shape and maximum deflection was thus fixed once the meshes were generated. Using appropriate blending functions makes it possible to control the span-wise location, lengths and maximum deflections of an arbitrary number of flaps via the input file to the flow solver. The span-wise blending function B_{span} was a simple piece-wise linear function where:

$$B_{span} = \begin{cases} 1 \, , R_{f-min} + \frac{\Delta R_f}{2} < r < R_{f-max} - \frac{\Delta R_f}{2} \\ \frac{1}{\Delta R_f} + \left(r - R_{f-min}\right) + 1 \, , R_{f-min} - \frac{\Delta R_f}{2} < r < R_{f-min} - \frac{\Delta R_f}{2} \\ \frac{-1}{\Delta R_f} + \left(r - R_{f-max}\right) + 1 \, , R_{f-max} - \frac{\Delta R_f}{2} < r < R_{f-max} + \frac{\Delta R_f}{2} \end{cases}$$

(2)

where r is the local radius, R_{f-min} and R_{f-max} are the minimum and maximum flap locations, and DR is the flap transition length. A second blending function was used to interpolate between the three mesh shapes according to the desired control surface deflection at each time step. At this stage the solver is capable of handling a prescribed analytical function to control the flap deflections or can be controlled through a discrete function read from a file. Extending the solver with feedback controls from e.g. a Pitot tube or strain-based sensors has been done in the 2D version of the solver (see [4]), and is planned to be included in the 3D solver in a continuation of this work.

All cases were run assuming fully turbulent flow, with the turbulence modeled using the K-w SST model [9]. To solve the pressure-velocity coupling the SIMPLE algorithm was used with six sub-iterations. The convective terms were discretized using the QUICK scheme. Case 1 and 2 were solved assuming steady state flow, since both cases involved only a static flap deflection. The remaining rotor simulation cases were all solved using the unsteady solver. A combination of grid sequencing and time step sequencing allowed for significant computational time savings. On the finest grid level a time step resulting in 3000 time steps per revolution was used. For a typical rotor simulation this resulted in a time step of approximately 0.0021 seconds.

The mesh around the NACA 64-418 profile section was generated as a 2D O-mesh using Hyp-Grid2D [15] and extruded in the span-wise

direction. Symmetry conditions were enforced in the span-wise direction. The mesh contained 256 cells in the chord-wise direction and 128 cells in the normal direction with 96 cells in the span-wise direction. To resolve the flap transition, the blade section at z=4.5 m to z=5.5 m was resolved with 32 cells resulting in a cell size of 0.031 m. The mesh was stretched towards the ends with a tangent hyperbolic function. Figure 1 shows the mesh around the profile.
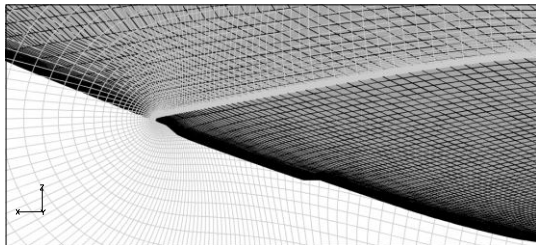
Figure 2 - *3D mesh around the NACA 64-418 blade section.*

Two types of meshes were generated for the NREL 5 MW Reference Turbine; One fully patched mesh with an O-O topology, and a mesh using overset grids, used in the non-uniform inflow cases. Fully patched mesh: The surface mesh had 256 cells in the chord-wise direction and 128 cells in the span-wise direction and was grown outwards using HypGrid3D to form an O-O topology. The first cell in the boundary layer had a height of 1×10−6 m corresponding to a $y+$ of less than 2. The outer boundaries of the domain were placed approximately eight rotor diameters away from the rotor. Figure 2 shows the overall domain and a detailed view of the mesh around the blade.
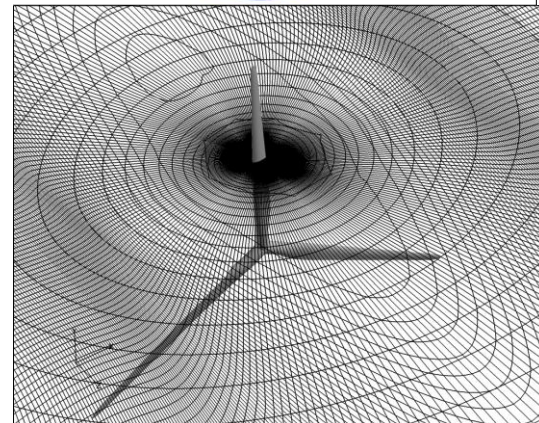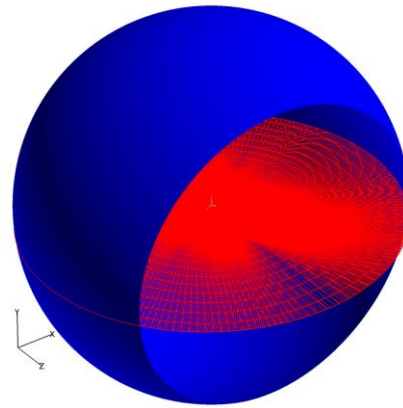
Figure 3 - Views of the overset mesh around the NREL 5MW reference turbine generated with a hub height of 90 m.

Overset mesh: This mesh consisted of four block groups: a rotor mesh, near-surface cylindrical mesh, a near-wake mesh, and a far-field mesh. The surface mesh was grown outwards approximately 7 m using 64 cells. This was embedded in a cylindrical mesh with a radius of 78 m and length of 34 m consisting of 96 blocks of 323 cells. The third block group covered the wake and had a radius of 88 m and extended 1.25 rotor diameters downstream and contained 80 blocks of 323 cells. The outermost block-group was semi-cylindrical and extended 8 rotor diameters away from the rotor and consisted of 52 blocks of 323. The total grid assembly contained 15×106 cells. Figure 3 shows a front-view and a side-view of the mesh.
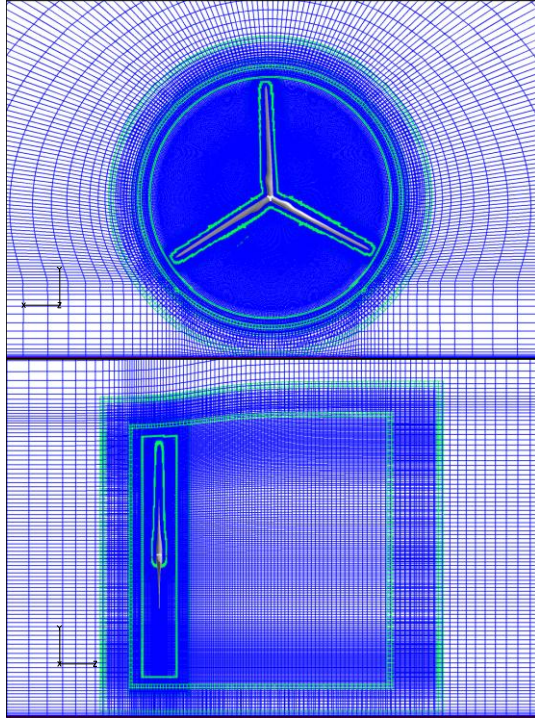
Figure 4 - Sideview and frontview of the overset mesh around the NREL 5MW reference turbine generated with a hub height of 90 m.

Figures 4 shows a close-up of the flapped region of the blade. Three meshes were generated, one with zero flap deflection and two with 10 deg upward and downward flap deflections, respectively.
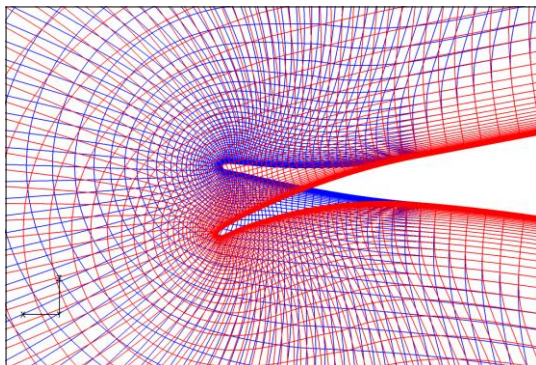
Figure 5 - Mesh around the NREL 5 MW reference turbine showing the meshes for the upward and downward deflected flaps.

3.2 HAWC2

The aeroelastic code HAWC2 [6] is utilized, modeling the full wind turbine configuration as a stiff structure. The aerodynamic forces are calculated using an unsteady Blade Element Momentum approach, including additional models for dynamic inflow, tip losses and azimuth-dependent induction. The calculation of local thrust and induction is performed in a polar grid using the local wind speed vectors. This improves predictions in case of non-uniform inflow like large shear and skew flow [8].The ATEFlap dynamic stall model [1,3,18] is included, which calculates the unsteady aerodynamics response of the airfoil sections with flaps based on provided static aerodynamic data. The static aerodynamic data is provided for the blade tip sections NACA64618 airfoil with a smooth 10% chord-wise length deformable trailing edge flap. The static data is generated using EllipSys 2D simulations, and the indicial response parameters for the attached-flow temporal response are obtained using the method in [19]. Based on the usual blade element formulation, the flap contribution to the local aerodynamic loads appears in distinct blade elements, without any modeled interaction between the flapped and non-flapped sections.
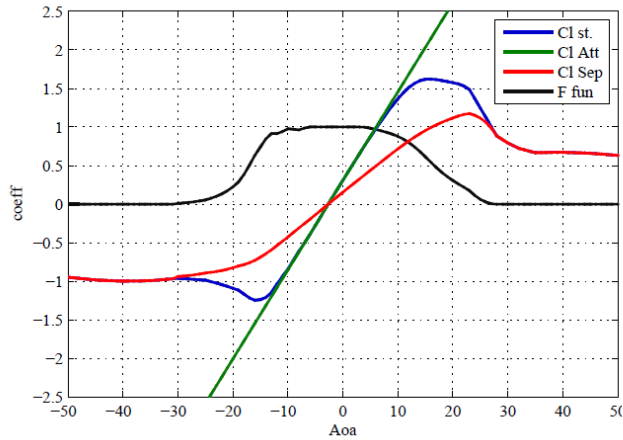
The ATEFlap model returns the dynamic lift, drag, and moment acting on an airfoil undergoing arbitrary motion and trailing edge flap deflection (arbitrary in the limits of the plane wake assumption). The dynamic effects reproduced by the model can be split into three categories. *Added mass* effects, or *non-circulatory* contributions, describe the forces that arise simply as a reaction of the fluid accelerated by the airfoil (or the flap) motion. The term has no memory effects, and only depends on the instantaneous motion of the airfoil or flap. Effects from *wake dynamics*, or *potential flow* effects, describe the memory effects of the vorticity shed into the wake, following a change of the airfoil aerodynamic loading, as, for instance, due to a variation in angle of attack or flap deflection. *Dynamic stall* effects represent the dynamics of the forces on an airfoil undergoing flow separation (stall).

The flow separation part of the model follows the Beddoes-Leishmann dynamic stall formulation
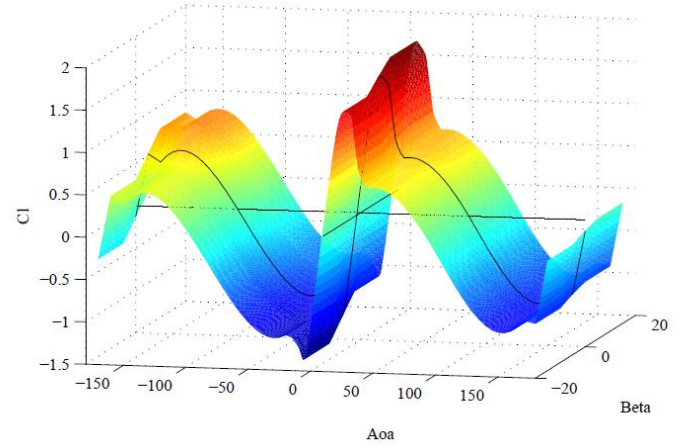
given in Hansen et al. [20]. The circulatory lift is expressed as a weighted sum of a fully attached and a fully separated contribution:

$$C_L^{c,dyn} = C_L^{att} f^{dyn} + C_L^{fs}\left(1 - f^{dyn}\right) \qquad (3)$$

The dynamics of the flow separation along the airfoil are described through the separation function f^{dyn}, which assigns the weight between the fully attached and the fully separated components. The value of the dynamic separation function is retrieved from the steady state function f^{st} evaluated at an equivalent angle of attack and flap deflection; the equivalent angle of attack and flap deflection values are determined from the lift coefficient returned by the potential flow part of the model. The steady Beddoes-Leishmann components giving the separation function f^{st}, the fully attached C_L^{att}, and fully separated C_L^{fs} lift coefficients are retrieved from the steady input data C_L^{st}. In the standard case of a cambered rigid airfoil, the operation is rather simple, and the Beddoes-Leishmann components are only function of the angle of attack. In the case of an airfoil with Adaptive Trailing Edge Flap, to account for the effects of the flap deflection, the steady lift C_L^{st} is a function of both angle of attack, and flap deflection β, Figure 2. The Beddoes-Leishmann components f^{st}, C_L^{att}, and C_L^{fs} also depend on both angle of attack, and flap deflection.

Figure 7 - Lift coefficient C^{st}_L in the case of an airfoil with trailing edge flap. The lift is a function of both angle of attack α and flap deflection β, and is a represented by a surface in space.

## 3.3 Test cases

Three control inputs are investigated, with:

- Flap angle based on a priori knowledge of the axial velocity from the analytical function defining the inflow velocity:

$$\delta = \delta_{max}\left(\tanh\left(8.78044\,\frac{x}{R}\right)\right) \qquad (4)$$

where x is the lateral coordinate in the rotor plane and R is the rotor radius.

- Flap angle based on feedback on Pitot tube velocity measured at the flap half-span. Individual flap command signal with proportional feedback on high-pass filtered (cut-off frequency f=0.05 Hz) resultant velocity at the mid-flap section (Kp=-1.3).
- Flap angle based on feedback on blade root flap-wise aerodynamic moment. Individual flap command signal with proportional feedback on high-pass filtered (cut-o_ frequency f=0.05 Hz) blade root flap-wise aerodynamic moment (Kp=0.0035).

Figure 6 - Steady lift coefficient curve as a linear combination of the steady components required by the Beddoes-Leishmann model: fully attached C^{st}_L and fully separated C^{fs}_L lift coefficients, weighted by the separation function f^{st} .

Figure 8 shows the flap signals of the three controls. The two feed- back controls are implemented in HAWC2 and the resulting flap signals are applied as prescribed input to the EllipSys3D simulations.
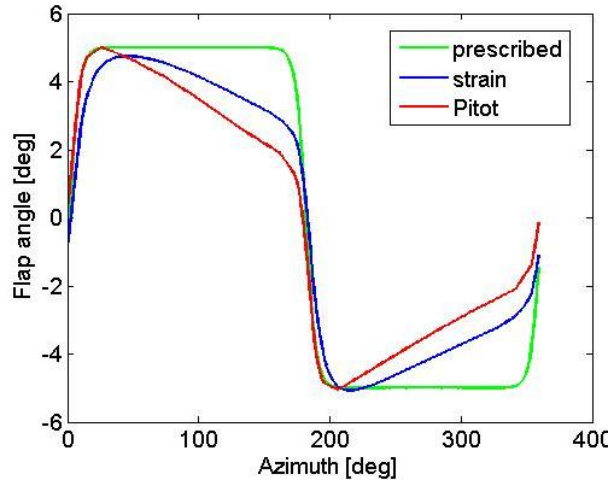
*Figure 8 - Flap angle signal for the three controls, for the case of maximum flap angles of ±5 deg.*

4. Results

The results for the investigated flap control cases predicted by EllipSys 3D and HAWC2 are presented and compared here.
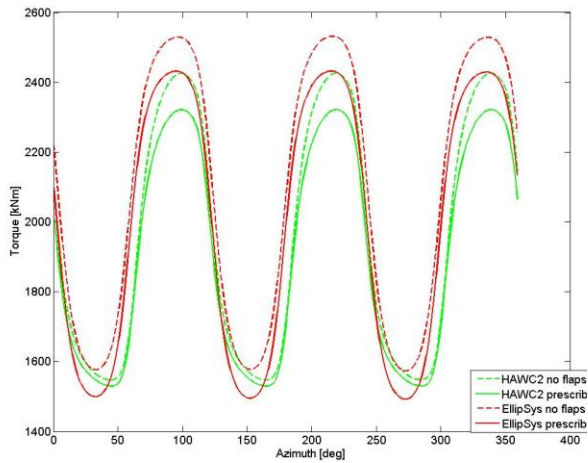
4.1 Prescribed flap angle control

Figures 3 and 4 show the rotor thrust and torque for the operation in half-wake with and without prescribed flap control. The maximum flap angle in this case is set to ±5 deg. For the simulations without flap control, there is reasonably good agreement between HAWC2 and EllipSys3D for this complex inflow situation. The capability of HAWC2 to predict such complex case can primarily be attributed to recent improvements in the unsteady inflow modeling in the code, where the local forces along the blades are now determined using fully localized induction factors and inflow velocities. HAWC2 predicts a longer delay in the response to the change in axial velocity than EllipSys3D as the blade passes from the low velocity 'wake' region to the

undisturbed inflow, corresponding to approximately 10 deg. azimuth phase delay. Additionally, there is an approximately 10% difference in the predicted minimum and maximum root moments for the two codes, which is evident in the thrust and torque predictions. The load reductions for the thrust and root bending moments are calculated as the percentage difference between the standard deviations of the loads with and without flap. For the torque the percentage difference is taken as the difference in mean levels. Looking at the two primary values, that of the thrust and blade root flap-wise bending moment, we observe that HAWC2 predicts a load reduction of 24.63% and 22.45%, respectively. EllipSys3D predicts significantly lower reductions of 14.43% and 17.31%, which is over 22% to 41% lower than predicted by HAWC2. Detailed results are presented in Table 1.
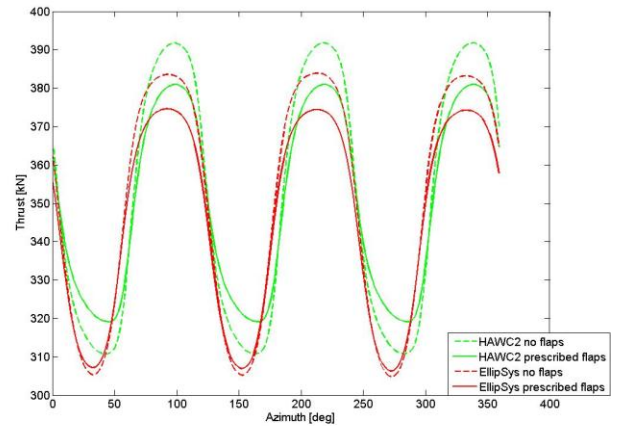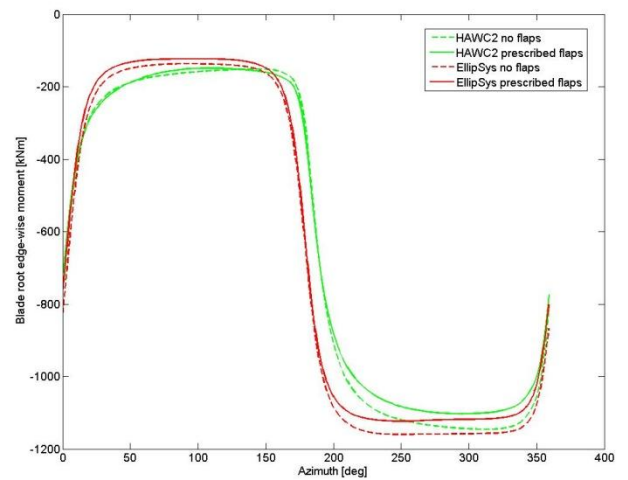

Figure 9 - Rotor thrust for the NREL 5MW reference turbine operating in half-wake with and without the prescribed flap control.
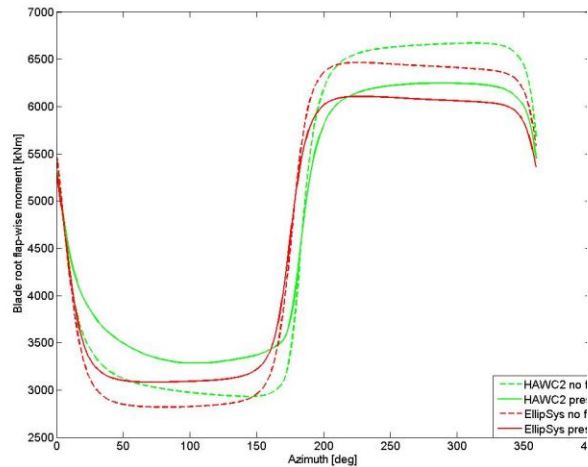
Figure 10 - Rotor torque for the NREL 5MW reference turbine operating in half-wake with and without the prescribed flap control.

Figure 12 – Blade root edge-wise bending moment for the NREL 5MW reference turbine operating in half-wake with and without the prescribed flap control.

*Table 1 – Results for the case of prescribed flap control*

	HAWC2			EllipSys		
	Std no flap	Std flap	Diff [%]	Std no flap	Std flap	Diff [%]
Thrust [kN]	32.00	24.12	24.63	30.22	25.86	14.43
Torque [kNm]	347.44	313.66	9.72	374.22	368.78	1.50
Mflap [kNM]	1688.20	1304.50	22.45	1652.80	1366.70	17.31
Medge[kNM]	442.96	422.37	4.65	466.13	456.09	2.15

Figure 11 – Blade root flap-wise bending moment for the NREL 5MW reference turbine operating in half-wake with and without the prescribed flap control.

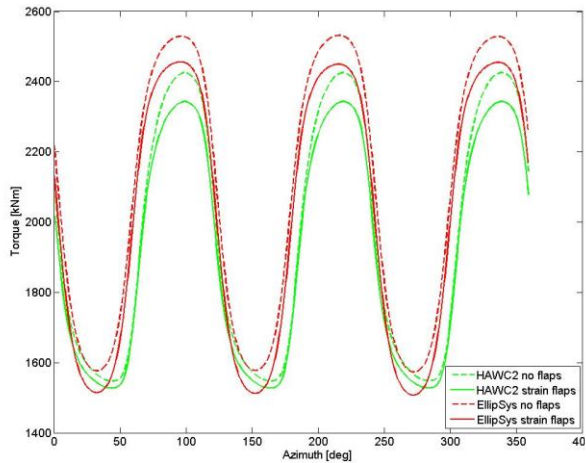## 4.2 Feedback flap angle control based on blade root flap-wise bending moment

In the second control type case, a feedback controller based on the blade root-ap-wise moment is used to set the flap angle. As shown in Figure 8, the maximum flap angle is as in the
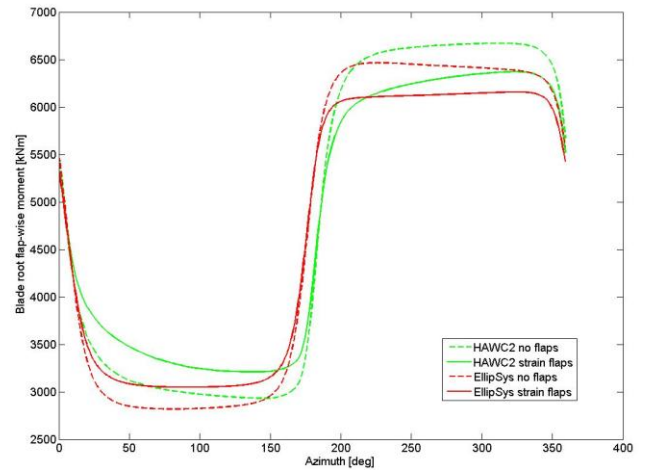
previous case 5 degrees. However, the flap signal differs quite significantly from the prescribed case, because of the use of the high-pass filter; in either of the two half-plane constant inflow regions, the high pass-filtered load signal moves towards a steady-state at zero. Detailed results are presented in Table 2.
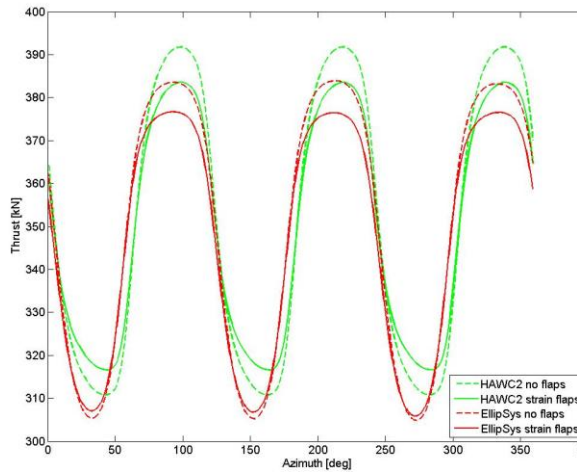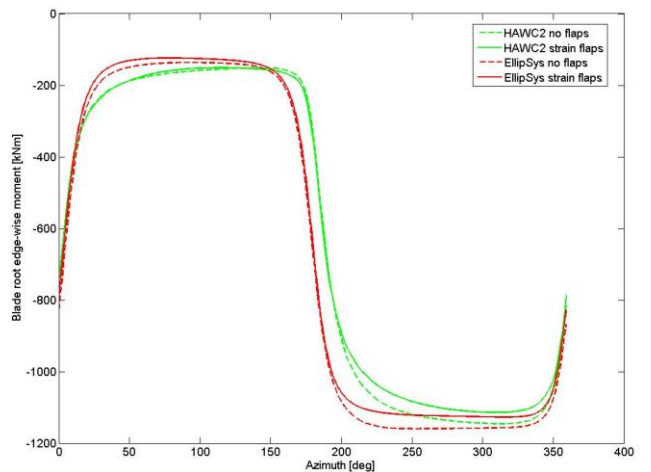

Figure 13 - Rotor thrust for the NREL 5MW reference turbine operating in half-wake with and without the feedback flap control based on blade root flap-wise bending moment.

Figure 15 – Blade root flap-wise bending moment for the NREL 5MW reference turbine operating in half-wake with and without the feedback flap control based on blade root flap-wise bending moment.

Figure 14 - Rotor torque for the NREL 5MW reference turbine operating in half-wake with and without the feedback flap control based on blade root flap-wise bending moment.
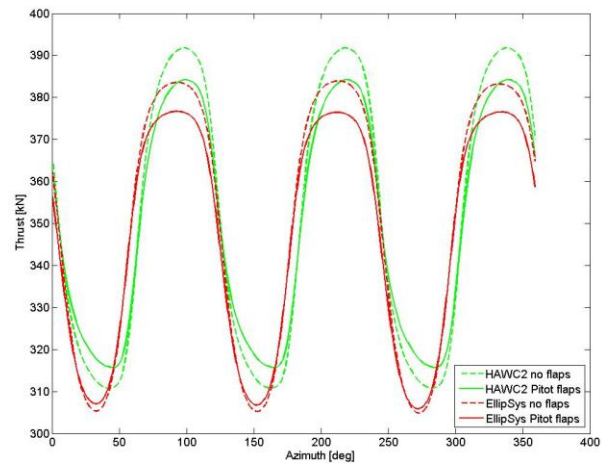

Figure 16 - Blade root edge-wise bending moment for the NREL 5MW reference turbine operating in half-wake with and without the feedback flap control based on blade root flap-wise bending moment

*Table 2 - Results for the case of feedback flap control based on blade root flap-wise bending moment*

	HAWC2			EllipSys		
	Std no flap	Std flap	Diff [%]	Std no flap	Std flap	Diff [%]
Thrust [kN]	32.00	26.44	17.37	30.22	27.15	10.15
Torque [kNm]	347.44	325.21	6.40	374.22	372.45	0.47
Mflap [kNM]	1688.20	1378.9	18.03	1652.80	1417.1	14.26
Medge[kNM]	442.96	426.87	3.63	466.13	457.50	1.85

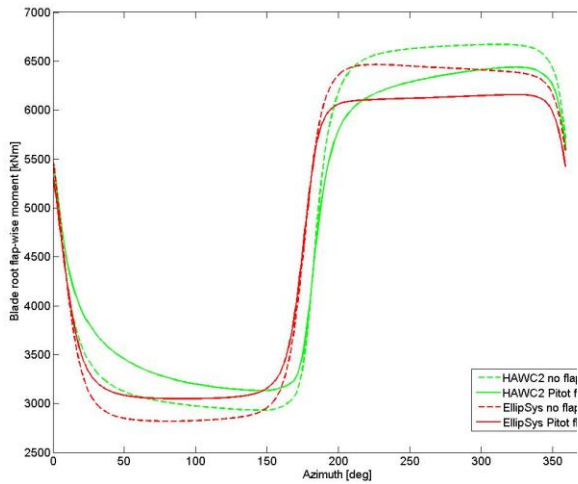## 4.3 Feedback flap angle control based on mid-flap location inflow

In the third control type case, a feedback controller based on the mid-flap velocity signal from an idealized Pitot tube is used to set the flap angle as shown in Figure 8, the maximum flap angle is again 5 degrees, in this case giving a faster response compared to the blade root moment signal. In the two feedback control cases the difference in the predicted load reductions between the two codes are consistent with the results for the prescribed flap angle results. In this case lower reductions are predicted compared to the idealized case where the flap angle is prescribed based on full knowledge of the inflow situation. It is also expected that using an inflow angle signal instead of a relative velocity signal will improve the flap response. Detailed results are presented in Table 3. The same flap signal as in the feedback to the blade root moment case was implemented in EllipSys, due to the small difference in the actual command signal.
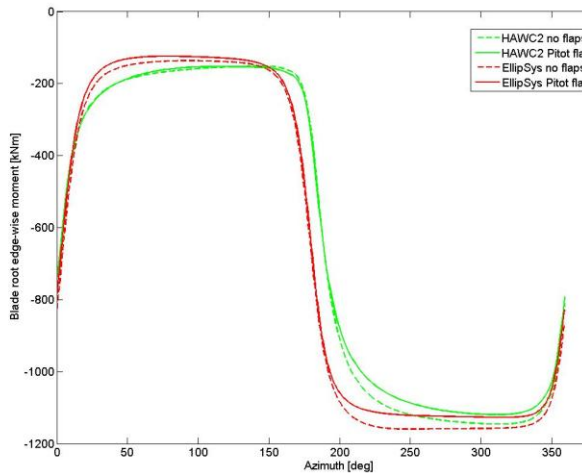

Figure 17 - Rotor thrust for the NREL 5MW reference turbine operating in half-wake with and without the feedback flap control based on mid-flap location inflow.
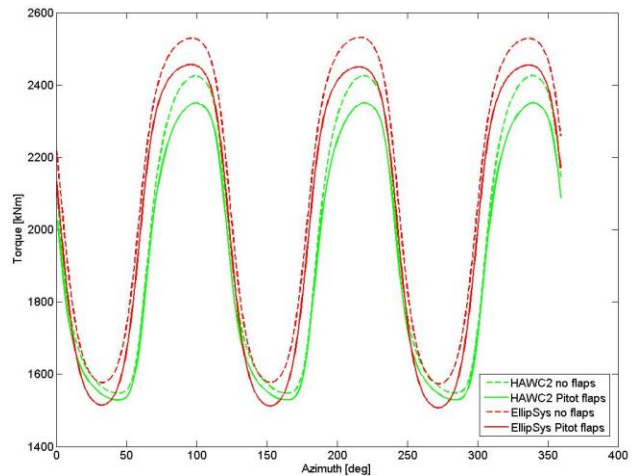
Figure 18 - Rotor torque for the NREL 5MW reference turbine operating in half-wake with and without the feedback flap control based on mid-flap location inflow.

Figure 19 - Blade root flap-wise bending moment for the NREL 5MW reference turbine operating in half-wake with and without the feedback flap control based on mid-flap location inflow.

Table 3 - Results for the case of feedback flap control based on mid-flap location inflow

	HAWC2			EllipSys		
	Std no flap	Std flap	Diff [%]	Std no flap	Std flap	Diff [%]
Thrust [kN]	32.00	26.76	16.37	30.22	27.15	10.15
Torque [kNm]	347.44	325.81	6.23	374.22	372.45	4.7
Mflap [kNM]	1688.20	1421.8	15.48	1652.80	1417.1	14.26
Medge[kNM]	442.96	428.53	3.26	466.13	457.50	1.85

4.4 Flowfield

A closer look at the flowfield (presented with contour plots of vorticity magnitude in Figures 21 and 22) reveals that the flow is highly complex due to the high loading of the rotor when passing through the low velocity half-wake region. This results in flow reversal downstream of the rotor, with a subsequent breakdown of the tip vortex. The high complexity of this flow case could also explain the discrepancies between the predicted load reductions with the two codes.

Figure 21 – Top view of the NREL 5MW reference turbine operating in half-wake with the prescribed flap control showing contours of vorticity magnitude in a horizontal plane through the rotor center – no flap.
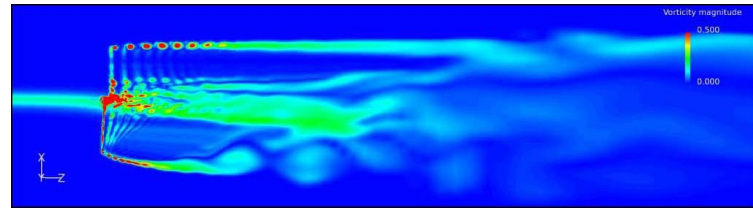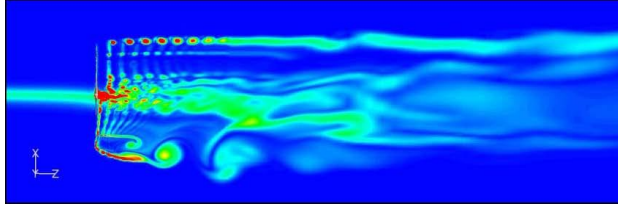

Figure 20 – Blade root edge-wise bending moment for the NREL 5MW reference turbine operating in half-wake with and without the feedback flap control based on mid-flap location inflow.

Figure 22 – Top view of the NREL 5MW reference turbine operating in half-wake with the prescribed flap control showing contours of vorticity magnitude in a horizontal plane through the rotor center – ±5 deg flap.

5. Conclusions

The newly implemented method to handle trailing edge flaps in EllipSys3D is demonstrated and found very stable and flexible allowing for an arbitrary number of flaps on each blade, with individual actuation of each flap. Generally, good agreement between the two codes is observed considering the complexity of this test case.

References

[1] P. Andersen. *Advanced Load Alleviation for Wind Turbines using Adaptive Trailing Edge Flaps: Sensoring and Control*. PhD thesis, RisøNational Laboratory, DTU, 2010.

[2] T. Barlas. *Active aerodynamic load control on wind turbines: Aeroservoelastic modeling and wind tunnel experiments*. PhD thesis, TUDelft, 2011.

[3] P. Andersen, M. Gauna, C. Bak, and M. Hansen. A dynamic stall model for airfoils with deformable trailing edges. *Wind Energy*, 12(8):734–751, 2009.

[4] J. Heinz, N. N. Sørensen, and F. Zahle. Investigation of the load reduction potential of two trailing edge flap controls using CFD. *Wind Energy*, 2010.

[5] R. I. Issa. Solution of the implicitly discretised fluid flow equations by operator-splitting. *Journal of Computational Physics*, 62:40–65, 1985.

[6] T. Larsen and A. Hansen. How 2 *HAWC*2, the user's manual. Technical Report Risø-R-1597(ver. 3 1)(EN), Risø, 2007.

[7] B. Leonard. A stable and accurate convective modelling procedure based on quadratic upstream interpolation. *Computer Methods in Applied Mechanics and Engineering*, 19:59–98, 1979.

[8] H. A.Madsen, V. Riziotis, F. Zahle,M. Hansen, H. Snel, F. Grasso, T. J. Larsen, E. Politis, and F. Rasmussen. Blade element momentum modeling of inflow with shear in comparison with advanced model results. *Wind Energy*, 2011.

[9] F. R. Menter. Zonal two-equation $k-w$ models for aerodynamic flows. *AIAA paper 93-2906*, 1993.

[10] J. A.Michelsen. Basis3D—a platform for development of multiblock PDE solvers. Technical Report AFM 92-05, Technical University of Denmark, 1992.

[11] J. A. Michelsen. Block structured multigrid solution of 2D and 3D elliptic PDEs. Technical Report AFM 94-06, Technical University of Denmark, 1994.

[12] S. V. Patankar and D. B. Spalding. A calculation procedure for heat, mass and momentum transfer in three-dimensional parabolic flows. *International Journal of Heat and Mass Transfer*, 15:1787–1806, 1972.

[13] C. M. Rhie and W. L. Chow. Numerical study of the turbulent flow past an aerofoil with trailing edge separation. *AIAA journal*, 21:1525–1532, 1983.

[14] N. N. Sørensen. General purpose flow solver applied to flow over hills. Technical Report Risø-R-827(EN), Risoe National Laboratory, 1995.

[15] N. N. Sørensen. HypGrid2D—a 2-Dmesh generator. Technical report, Risø-R-1035(EN), Risoe National Laboratory, 1998.

[16] F. Zahle. *Wind Turbine Aerodynamics Using an Incompressible Overset Grid Method.* PhD thesis, Imperial College, London, 2006.

[17] J. Jonkman. *Wind Definition of a 5-MW reference wind turbine for offshore system development.* Technical Report, NREL, NREL/TP-500-38060, 2009.

[18] L.Bergami and M. Gaunaa. ATEFlap aeordynamic model, a dynamic stall model including the effects of trailing edge flap deflection. Technical Report, R-1792(EN), Risø National Laboratory. Technical University of Denmark, 2011.

[19] L. Bergami and M. Gaunaa, and Joachim Heinz. 'Indicial Lift Response Function: An Empirical Relation for Finite-thickness Airfoils, and Effects on Aeroelastic Simulations'. Wind Energy, in-press .

[20] M. H. Hansen, M. Gaunaa, and H. A. Madsen. A Beddoes-Leishman type dynamic stall model in state-space and indicial formulations. Technical Report, Risø, Risø-R-1354(EN).

[21] H. A. Madsen, V. Riziotis, F. Zahle, M. O. L. Hansen, H. Snel, F. Grasso, T. J. Larsen, E. Politis and F. Rasmussen, Blade element momentum modeling of inflow with shear in comparison with advanced model results. *Wind Energy*, published online, DOI: 10.1002/we.493, 2011.